Fuel Processing Technology 152 (2016) 390–398

Contents lists available at ScienceDirect

Fuel Processing Technology

journal homepage: www.elsevier.com/locate/fuproc

# Thermophysical properties of the marine microalgae *Nannochloropsis salina*☆

Nico Schneider [a,*], Tara J. Fortin [b], Roland Span [a], Mandy Gerber [c]

[a] Ruhr-Universität Bochum, Lehrstuhl für Thermodynamik, Universitätsstr. 150, 44801 Bochum, Germany
[b] National Institute of Standards and Technology, Applied Chemicals and Materials Division, 325 Broadway MS 647.07, Boulder, CO 80305, USA
[c] Hochschule Bochum, Institut für Thermo- und Fluiddynamik, Lennershofstr. 140, 44801 Bochum, Germany

ARTICLE INFO

*Article history:*
Received 24 March 2016
Received in revised form 24 June 2016
Accepted 28 June 2016
Available online 15 July 2016

*Keywords:*
Microalgae
Density
Viscosity
Isobaric heat capacity
Temperature
Total solid content

ABSTRACT

Algae have a variety of uses, including pharmaceutical and cosmetic products, and as a potential energy source as a feedstock for biodiesel, bioethanol and biogas. To optimize the commercial production and use of algal biomass, production facilities have to be specifically designed to handle the source materials and subsequent products. This requires a knowledge of their thermophysical properties. To that end, density, viscosity, and heat capacity of the marine microalgae *Nannochloropsis salina* were determined experimentally at atmospheric pressure and as a function of temperature and total solid (TS) content. Correlation analyses show a relationship between experimental data, temperature, and total solid content for each of the investigated thermophysical properties. Thus, equations were developed allowing the calculation of these properties as a function of temperature and TS content.



## 1. Introduction

Algae are found in a variety of pharmaceutical, cosmetic, and food products [1]. Currently, there are efforts to provide energy from algal biomass in the form of biodiesel, bioethanol, biogas, hydrogen, and synthetic gas due to its advantages over fossil fuels and other energy crops [2]. For example, the use of algal biomass as a renewable and sustainable energy source results in reduced greenhouse gas emissions relative to fossil fuels. Moreover, the cultivation of algae does not require arable lands and, therefore, does not compete with edible crops [3]. Finally, algae have higher growth rates than terrestrial plants allowing for the continuous harvesting of biomass throughout the whole year [4].

During cultivation, harvesting, and downstream processing, algal biomass can be classified as a complex suspension. It consists of a liquid water phase and a solid phase that includes polymers derived from biological organisms, dispersed algal cells, dissolved salts, and insoluble solids [5,6]. However, the relative concentrations of the liquid and solid phases change during the processing of algal biomass. Prior to harvesting, the water content of algae is usually higher than 99% by mass, even in cultivation systems with high cell densities [7]. Harvesting techniques are classified as either primary or secondary. Primary harvesting systems incorporate sedimentation and flotation technologies which separate the algal cells from their growth media resulting in an algal slurry with a total solid (TS) content between 0.5% and 6% [7]. Further thickening is achieved by secondary harvesting, which utilizes technologies like a centrifuge or a belt press and leads to a TS content between 10% and 20% depending on the intended final application [7]. In general, the cultivation of most microalgae species requires temperatures between 293 K and 303 K [4,8]. Since commonly used harvesting methods do not require heating or cooling of the algal biomass, the harvesting is also done at ambient temperatures.

To optimize the commercial production and use of algal biomass, production and downstream processing facilities have to be specifically designed to handle the source materials and subsequent products. For instance, microalgae-based energy production requires multiple processing steps (e.g., dewatering, drying, pumping, etc.); substance specific design and dimensioning of the equipment involved at each of these steps (e.g., pumps, mixers, heat exchangers, etc.) is necessary to increase processing efficiency [3,6,8]. This requires a knowledge of thermophysical properties such as density, viscosity, and heat capacity. However, such data are rarely found in the relevant literature on algal biomass. Regarding density, most studies deal with the optical or cell density of algae, which is different from the volumetric mass density. The situation is improved regarding the rheological behavior of algal biomass, which includes viscosity. Several studies have shown a dependence of the viscosity on both the temperature and the TS content of algal biomass for microalgae species such as *Chlorella* sp. [6,9], *Nannochloropsis* sp. [5] and *Chaetoceros muelleri* [10], among others. Additionally, a change from Newtonian to non-Newtonian fluid behavior with increasing TS content has been observed for algal slurries (e.g. [11–13]). However, none of these studies present an equation to allow

☆ Contribution of the National Institute of Standards and Technology. Not subject to Copyright © in the U.S.A.

* Corresponding author.
*E-mail address:* N.Schneider@thermo.rub.de (N. Schneider).

http://dx.doi.org/10.1016/j.fuproc.2016.06.039
0378-3820/

for the calculation of viscosity as a function of temperature and TS content. Previously, Schneider and Gerber [14] presented a correlation equation for the viscosity of untreated, thermally-pretreated and digested *Nannochloropsis salina* biomass over a limited TS content range as a function of temperature. Correlation equations to calculate the density or heat capacity of algal biomass as a function of temperature and TS content are not available in the relevant literature.

The main objective of this study was to develop correlation equations to allow for the calculation of density, viscosity and heat capacity as a function of temperature and TS content for the full technically relevant TS content range. To that end, these properties were determined experimentally at atmospheric pressure (~83 kPa in Boulder, CO) and as a function of temperature and TS content for the marine microalgae *Nannochloropsis salina* (*N. salina*), which is a commonly used algae species, especially in the production of biodiesel, fish feed and pharmaceuticals due to its high growth rates and lipid productivity [15]. The experimental data, as well as the resulting correlation equations are presented herein.

## 2. Material and methods

### 2.1. Algal biomass

Biomass from the marine microalga *N. salina* was obtained from BlueBioTech GmbH (Büsum, Germany).[1] The algae culture was grown in a greenhouse in an airlift reactor at 296 to 298 K and a pH of 8.3 in standard F medium at a salinity concentration of 32 ppt. Algal sludge was harvested via continuous centrifuge. The supernatant of the centrifugation process was used to resuspend the biomass to the desired concentration (TS content of ~23%). Two external laboratories were enlisted to help further characterize the undiluted algal sample. Organic composition (raw protein, raw fat, raw ash, raw fiber, raw carbohydrate) was determined by Warren Analytical Laboratory (Greeley, CO, USA)[1] via a proximate, or Weender, system analysis [16]. Elemental composition (C, H, N, S, O) was analyzed by Midwest Microlab LLC (Indianapolis, IN, USA)[1]. In their analysis, C, H, N, and S were determined analytically and O was calculated assuming those five elements accounted for 100% of the organic composition.

Samples of various TS content were prepared by diluting the algal biomass with appropriate aliquots of distilled water. No changes in the cell walls were observed as a result of these dilutions (see Supporting Information). The TS content of each sample was analyzed according to DIN EN 12880 [17] with each determination being performed in triplicate. Specifically, 7.605 ± 1.412 g of sample were weighed out into crucibles using an analytical balance (weighing range: 110 g; readability: 0.001 g; linearity: 0.002 g; repeatability: 0.001 g). The samples were dried in an oven at 378.15 K for about 12 h; the reported TS content represents the amount of solids remaining after drying.

Particularly for the density measurements, samples needed to be free of gas bubbles to obtain reliable results. Therefore, all samples were degassed prior to use with multiple cycles of freezing, evacuating the vapor space over the frozen sample, and thawing. In between measurements, the samples were kept cold by storing them in a refrigerator.

Measurements were made at temperatures ranging from an overall minimum of ~293 K to an overall maximum of ~333 K. Since most relevant technical applications dealing with the cultivation, harvesting and downstream processing of algal biomass operate at ambient conditions, ambient temperature was used as the lower limit. The upper limit was chosen to make sure that the investigated properties were not influenced by a change in cell structure, agglomeration of cells, or cell wall damage due to the heating of the samples during experiments (see Supporting Information for additional information).

### 2.2. Density measurements

A commercial density and sound speed analyzer was used to measure the density in 5 K steps over the temperature range from 293.15 K to 333.15 K and at ambient pressure (~83 kPa). Typically, density and speed of sound are measured simultaneously with this instrument but for this work only density was measured; the use of a special inlet adapter made it possible to bypass the sound speed cell and inject sample directly into the density cell. In this instrument, density is measured with a vibrating tube densimeter that is housed in a thermostated copper block whose temperature is controlled via thermoelectric Peltier elements and a Pt-100 resistance thermometer. Prior to use, the instrument was calibrated with deionized water and air; toluene standard reference material (SRM) 211d was used to validate the performance of the calibrated instrument. At least three temperature scans were performed for each concentration with fresh sample injected into the instrument prior to each measurement run. In between samples, the density cell was carefully cleaned to avoid cross-contamination; cleanliness was verified with measurements of water at 293.15 K, otherwise known as a water check. Additional details on the apparatus and experimental procedures can be found in Fortin [18], Laesecke et al. [19], and Fortin et al. [20].

### 2.3. Viscosity measurements

A falling-needle rheometer was used to measure the viscosity of the algal biomass. It was developed by Yamamoto and coworkers to measure the rheological properties of fresh human blood without anticoagulant [21,22] and belongs to the class of falling ball and cylinder viscometers [23–25]. It can be used for Newtonian as well as non-Newtonian fluids. The apparatus, its function, and a schematic of the set up were described in detail by Yamamoto et al. [21] and Burger et al. [26]. Thus, only a brief description will be given here.

The rheometer consists of two vertical cylinders. The inner cylinder is filled with the sample and is placed concentrically within an outer cylinder. The space between the two cylinders is filled with circulating temperature-controlled water to regulate the sample temperature. To determine the fluid viscosity, a slender hollow cylinder with hemispherical ends (the needle) is dropped through the sample. To ensure that the longitudinal axes of the fluid vessel and the needle are parallel to the gravity vector and to guide the needle to the center of the fluid sample, a needle inlet and a launcher are located at the top of the inner cylinder. The time it takes for the needle to pass between two magnetic sensors located in the middle section of the cylinders is measured automatically and recorded electronically by a programmable controller. From the elapsed time, the fall velocity can be calculated and then used to determine shear rate, shear stress, and hence the viscosity of the fluid via a flow analysis. Details on the mathematical models used and the flow analysis can be found in Burger et al. [26] and Yamamoto et al. [21].

To generate a variety of shear rates and shear stresses, several needles with varying densities were used. The density of each needle is determined by the mass of an enclosed metal sinker that is fixed at the bottom of each needle cylinder. For each TS concentration, five measurement runs were carried out at each temperature and for each run at least eight needles were dropped. Measurements were made over the temperature range from 293.15 K to 323.15 K and at ambient pressure (~83 kPa). For these measurements, a thermocouple (estimated uncertainty 0.25 K) was used to measure the sample temperature before and after each measurement run.

[1] Certain trade names are identified only to adequately describe materials and experimental procedures. This does not constitute a recommendation or endorsement of these products by the National Institute of Standards and Technology, nor does it imply that the products are necessarily the best available for the purpose.

### 2.4. Heat capacity measurements

A commercial modulated differential scanning calorimeter (MDSC) was used to measure the isobaric heat capacity of the algae samples. In conventional DSC, the difference in heat flow between a sample and an inert reference is measured as a function of time and temperature while both are subjected to a controlled environment. What is different with MDSC is the heating profile applied; in DSC, a simple linear profile is utilized, but in MDSC, a sinusoidal modulation is overlaid on the conventional linear heating ramp. The net effect is equivalent to performing two experiments simultaneously, one experiment at the average linear heating rate and a second at an instantaneous sinusoidal heating rate. In addition, while it is only possible to measure total heat flow with conventional DSC, with MDSC it is possible to separate total heat flow into its two components: one that is a function of the sample's heat capacity and rate of temperature change (the heat capacity or "reversing" component) and one that is a function of the absolute temperature and time (the kinetic or "nonreversing" component). The combined net effect of these two advantages is a simpler, more precise measurement of heat capacity with MDSC compared to conventional DSC. Additional details regarding MDSC theory can be found in Reading et al. [27] and Wunderlich et al. [28]. In this work, measurement runs were performed from 278.15 K to 338.15 K using an underlying heating rate of 3 $K \cdot min^{-1}$ and modulated conditions of $\pm 1$ K every 120 s. The sample cell was continuously purged with a 50 $mL \cdot min^{-1}$ flow of dry nitrogen.

Determination of accurate heat capacities with both DSC and MDSC requires calibration of temperature, heat flow, and heat capacity. Temperature and heat flow are calibrated via measurements of materials with known transition temperatures and heats; in this work, adamantane, indium, and tin were used. Indium SRM 2232 and tin SRM 2220 were obtained from the National Institute of Standards and Technology (NIST) and corresponding reference melting temperatures and heats of fusion were obtained from their respective certificates [29,30]. Adamantane was not available as a certified reference material. The adamantane sample used was obtained from Sigma-Aldrich with a stated purity of >99%. Our own analysis by gas chromatography/mass spectrometry indicated a purity of >99.95%. The adamantane was used without further purification, and reference values for the temperature and heat of transition for the first order solid-solid transition were taken from Westrum [31]. Heat capacity was calibrated by measuring sapphire ($Al_2O_3$) under the same experimental conditions as were used for the algae samples and comparing measured specific heat capacities to literature values [32]. Temperature and heat flow calibrations were performed prior to start of algae measurements, and the calibration was validated daily via a single indium measurement. Heat capacity calibrations were performed before and after every algae sample run; an overall average of the thirty-five separate sapphire calibration runs was used to calculate the temperature-dependent calibration constant to apply to each algae sample.

All calibration and algae samples were encapsulated in hermetically sealed aluminum pans. An empty sealed pan served as the reference. At least three pans were prepared for each measured TS concentration. Algae sample masses ranged from 4.21 mg to 21.67 mg; multiple masses were measured to check for any evidence of mass dependence, which would indicate a significant contribution from the vapor phase. Pans were weighed before and after measurements to check for sample loss; mass changes of >0.3% would require data to be discarded. No samples had to be discarded as a result of sample loss in this work. Each pan was measured in triplicate, resulting in a total of at least nine measurement runs for each TS concentration measured.

**Table 1**
Averaged total solid (TS) content (±standard deviation) of the measured samples and the results of organic and elemental composition analyses of *Nannochloropsis salina*.

| | | | |
|---|---|---|---|
| TS content of the measured samples | % of FM[a] | 20.33 ± 0.02 | 9.62 ± 0.01 |
| | | 17.74 ± 0.03 | 7.88 ± 0.03 |
| | | 15.98 ± 0.02 | 5.33 ± 0.03 |
| | | 13.44 ± 0.02 | 2.92 ± 0.00 |
| | | 10.95 ± 0.01 | 1.42 ± 0.01 |
| Crude protein | % of TS | 24.53 | |
| Crude fat | % of TS | 42.60 | |
| Crude fiber | % of TS | 1.56 | |
| Nfe | % of TS | 18.18 | |
| Crude ash | % of TS | 13.13 | |
| C | % of TS | 55.11 | |
| H | % of TS | 7.63 | |
| N | % of TS | 6.02 | |
| S | % of TS | 0.33 | |
| O | % of TS | 17.78 | |

[a] FM = fresh matter.

## 3. Results and discussion

### 3.1. Sample composition

The TS content of the samples measured in this work can be found in Table 1. TS contents range between 1.42 ± 0.01% and 20.33 ± 0.02%, which are commonly found TS contents in practice. There, the specific TS content of algae biomass mostly depends on the particular harvesting process used; an overview can be found in Christenson and Sims [33].

To further characterize the microalgal biomass, its organic and elemental composition were analyzed. The results of the analyses are presented in Table 1. All reported values for the organic and elemental composition are within the same order of magnitude as results reported for other batches of *N. salina* biomass provided by the same manufacturer [14,34]. Thus, it seems reasonable to assume that the thermophysical property results reported herein are representative of other batches of the same microalgae species. However, the applicability to other microalgae species needs to be experimentally tested and verified.

### 3.2. Density

Table S2.1 in the Supporting Information summarizes the results of density measurements including corresponding expanded uncertainties. Reported density values are averages of replicate measurements. To determine the expanded uncertainty, $U(\overline{\rho})$, for each average density, $(\overline{\rho})$, a detailed uncertainty analysis was carried out. The combined standard uncertainty, $u(\overline{\rho})$, is defined as follows:

$$u(\bar{\rho}) = \sqrt{\frac{1}{n}s_\rho^2 + u^2(c) + u^2(\gamma) + u^2(t)} \quad (1)$$

where $s_\rho$ is the standard deviation of the average of $n$ values; $u(c)$ is the uncertainty contribution from the instrument calibration estimated from pre- and post-measurement water runs, $u(\gamma)$ is the uncertainty contribution from the instrument resolution, and $u(t)$ is the contribution due to the uncertainty in the measured temperature. Once $u(\overline{\rho})$ has been calculated, the Welch-Satterthwaite approximation [35] can be used to calculate the effective degrees of freedom, $(df)$, which are used to determine the appropriate coverage factor, $k(df)$, from a t-distribution for a 95% confidence level. $U(\overline{\rho})$ is than calculated as

$$U(\overline{\rho}) = k(df) \cdot u(\overline{\rho}). \quad (2)$$

Additional details regarding the uncertainty analysis can be found in Fortin [18] and Fortin et al. [20]. Overall, expanded uncertainties range between 0.66 $kg \cdot m^{-3}$ and 0.72 $kg \cdot m^{-3}$ (0.064% to 0.070%).

As can be seen in Fig. 1a, the density of the algal biomass depends on temperature and TS content. Specifically, the density increases almost linearly with increasing TS content but decreases with increasing temperature. It is unclear why the densities at 15.81% and 17.96% TS are so close together.

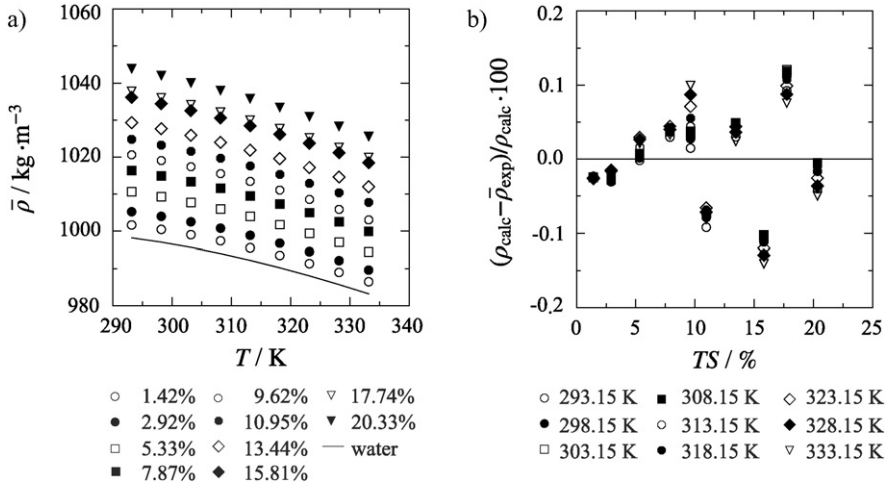


**Fig. 1.** Density results: a) averaged experimental results ($\bar{\rho}$) for measured TS concentrations plotted as a function of temperature ($T$) and water density calculated using the IAPWS-95 formulation of Wagner and Pruss [39] and, b) percent deviations for experimental data relative to densities calculated using Eq. (3).

No equation relating algal biomass density to temperature and TS content could be found in the literature. In contrast, equations based on these parameters are available for liquid foods like fruit purees, juices, or milk (e.g. [36–38]). In most cases, a simple polynomial equation yields sufficient results. However, only the amount of soluble solids is typically considered instead of the TS content, which also includes insoluble solids. Furthermore, those equations do not account for the fact that the samples are essentially water at a TS concentration of 0%. Fortunately, this can be remedied since Wagner and Pruss [39] have published an accurate fundamental equation of state that can easily be used to calculate the density of water at any temperature of interest. Taking the above points into consideration, a numerically stable but accurate polynomial approach was chosen here, which resulted in an empirical equation to calculate the density of *N. salina* biomass as a function of temperature and TS content:

$$\rho(T,TS) = \rho_{H_2O}(T) + a_\rho \cdot T^{b_\rho} \cdot \left( c_\rho \cdot \left(\frac{TS}{100}\right)^{d_\rho} + e_\rho \cdot \left(\frac{TS}{100}\right)^{f_\rho} \right) \quad (3)$$

where $\rho$ is the density in $kg \cdot m^{-3}$, $T$ is the temperature in K, $TS$ is the total solid content in %, and $\rho_{H2O}(T)$ is the density of water in $kg \cdot m^{-3}$ and at a temperature $T$ in K and at atmospheric pressure calculated with the IAPWS-95 formulation by Wagner and Pruss [39]. Using this equation structure, the density for a TS content of 0% is equivalent to the density of pure water. For the adjustment of the equation parameters, the weighted sum of squares was reduced by a Newton-Raphson method. During the fitting procedure it was important to not only reproduce the experimental data as well as possible but also for the equation to maintain a reasonable physical behavior.

The experimental data in Table S2.1 (see Supporting Information) were fit with Eq. (3); the resulting coefficients ($a_\rho$, $b_\rho$, $c_\rho$, $d_\rho$, $e_\rho$ and $f_\rho$) can be found in Table 2. The resulting relative deviations between experimental and calculated densities are presented in Fig. 1b, 95% of the data are found in the range between −0.14% and 0.12%.

No systematic trends are observed in the deviations shown in Fig. 1b. To further investigate the robustness of Eq. (3), its extrapolation behavior is plotted for a TS content range from 0% to 30% (Supporting Information, Fig. S3.1a) and for a temperature range from 274 K to 365 K (Supporting Information, Fig. S3.1b). It is clear from both figures that the equation exhibits normal trends without any unusual variations.

### 3.3. Viscosity

Based on the measured needle fall velocities, shear stress ($\tau$), shear rate ($\dot{\gamma}$), and viscosity ($\eta$) were calculated according to the model of Yamamoto et al. [21]. The model assumes that the analyzed fluid is Newtonian. For Newtonian fluids, the constitutive equation

$$\tau = \eta \cdot \dot{\gamma} \quad (4)$$

is used to calculate the viscosity. For non-Newtonian fluids the values calculated by Eq. (4) represent apparent or effective viscosities ($\eta_{eff}$).

Fig. 2 shows the corresponding viscosities and effective viscosities as a function of shear rate for 15.81% and 17.74% TS contents at 323.15 K. Data are not shown for the other temperatures and TS contents since the curves look similar to those shown for these two representative TS contents. Flow curves (shear stress as a function of shear rate) of the samples with TS contents up to 15.81% show that the shear stress linearly depends on the shear rate for the investigated temperatures, indicating Newtonian behavior. Thus, the resulting viscosities are independent of the shear rate (see Fig. 2) and can be averaged over the whole shear rate range. Table S2.2 (see Supporting Information) summarizes the averaged viscosities for the Newtonian behaving concentrations, as well as their corresponding expanded uncertainties. Expanded uncertainties were calculated in a manner analogous to that previously described for density (Section 3.2). The combined standard uncertainty for viscosity incorporates the standard deviation of the average of $n$ measurements, as well as uncertainty contributions associated with the calibration of the falling needle rheometer, the needle density, the sample density and the temperature. For the calculation of the expanded uncertainty $U(\bar{\eta})$, a coverage factor $k(df) = 2$ was used. Overall, the expanded uncertainties for the samples showing Newtonian behavior range between 0.07 mPa·s and 0.92 mPa·s (5.79% to 6.13%).

For TS contents of 17.74% and 20.33%, the resulting flow curves show a non-linear dependence of shear stress on shear rate. Furthermore, the effective viscosity decreases with increasing shear rate (Fig. 2). This is indicative of non-Newtonian, shear-thinning behavior. The averaged shear rates, averaged effective viscosities, and corresponding expanded uncertainties are summarized in Table S2.3 (see Supporting Information) for the two TS concentrations exhibiting this non-Newtonian behavior. The expanded uncertainties were calculated using the same approach and the same coverage factor as was previously described

for the samples exhibiting Newtonian behavior. Here, the expanded uncertainties range between 0.87 mPa·s and 1.81 mPa·s (5.78% to 6.43%).

Fig. 3a shows the averaged viscosities for algae samples exhibiting Newtonian behavior as a function of TS content and temperature. The viscosity of water was calculated at experimental temperatures and atmospheric pressure using the IAPWS formulation of Huber et al. [40] and the results are shown in Fig. 3a for comparison. Fig. 3b shows the effective viscosities as a function of shear rate and temperature for 17.74% and 20.33% TS content. It is clear from Fig. 3a and b that the viscosity increases with increasing TS content and decreases with increasing temperature. According to Barnes [41], an increasing concentration of the dispersed phase results in an increase in the viscosity of a suspension due to the irreversible dissipation of mechanical energy caused by the divergence of the streamlines around the particles in the suspension. Thus, a higher total solid content with its greater concentration of algae cells and polymeric substances results in an increase in viscosity.

The decrease in viscosity with increasing temperature is more consistent than the dependency on TS content. For example, for the 9.62% TS content sample, a temperature rise of 10 K from 303.15 K to 313.15 K leads to a decrease in viscosity of approximately 13% (3.841 to 3.344 mPa·s). Another 10 K rise results in another decrease of approximately 13% (3.340 to 2.887 mPa·s). The same temperature dependence is observed for the non-Newtonian samples.

In contrast, Fig. 3a clearly shows that the viscosity increases non-linearly with increasing TS content. For instance, an increase of approximately 50% of the TS content (from 5.33% to 7.88%) leads to an increase in viscosity of approximately 40% (2.465 to 3.430 mPa·s), whereas an increase of approximately 100% of the TS content (from 5.33% to 10.95%) results in a viscosity increase of almost 145% (2.456 to 6.035 mPa·s).

The observed transition from Newtonian behavior at lower concentrations to non-Newtonian, shear-thinning behavior at higher concentrations has been observed in other studies on the rheological behavior of different microalgae suspensions. For example, Zhang et al. [9] and Santos et al. [6] investigated the fluid behavior of *Chlorella* sp. suspensions and observed a similar change in rheological behavior with algae concentration. Similar results have also been observed for suspensions of *Nannochloris* sp. [5], *Haematococcus lacustris* [11], *Scenedesmus obliquus* [12], *Chaetoceros muelleri* [10], *Chlorella pyrenoidosa* [42], and *Chlorella vulgaris* [13]. However, in most of these cases, the effect occurred at much lower concentrations than what is observed in this work. In addition to the rheological behavior, Souliès et al. [13] also used microscopy to investigate the distribution and size of microalgae cells in the *Chlorella vulgaris* suspensions and found that no clusters of cells (or solids) could be observed at low concentrations. However, they observed that with increasing concentration the larger cells tended to group together and started to form cell aggregates, or flocs. Consequently, they attributed the observed shear-thinning behavior to the formation of flocs at certain cell concentrations. Similar results were previously reported by Adesanya et al. [12] for suspensions of *Scenedesmus obliquus*. They concluded that flocs formed as a result of intermolecular forces of attraction (e.g., van der Waals forces) and caused shear-thinning behavior at higher concentrations.

Although studies reporting rheological behavior and viscosity dependence on temperature and TS content exist in the literature (e.g. [5,12]) equations allowing for the calculation of viscosity based on those parameters do not. Only equations for the thermophysical properties of liquid foods are available. For example, Gabas et al. [38] and Fernández-Martín [43] report equations for the calculation of the viscosity of different milks. Gabas et al. [38] used an Arrhenius-type equation to describe the temperature dependence and extended it to include the dependence on TS content. The resulting exponential equation led to deviations of approximately 7.76% between experimental and calculated values for Newtonian samples. Fernández-Martín [43] constructed a logarithmic function with a polynomial dependence on temperature and TS content, which led to deviations within 5%. The author further reports that at 0% TS content the equation showed good agreement with the viscosity values for pure water. However, neither of the above equations explicitly account for the viscosity of water at 0% TS content, which can be readily done using the IAPWS formulation of Huber et al. [40]. Here, a numerically stable but accurate exponential approach was chosen. Empirical equations have been developed to calculate the viscosity of *N. salina* biomass as a function of temperature and TS content, which incorporate the viscosity of water at 0% TS content. Separate equations were developed for each of the two observed rheological regions. For the Newtonian region with TS contents up to 15.81% the following equations are used:

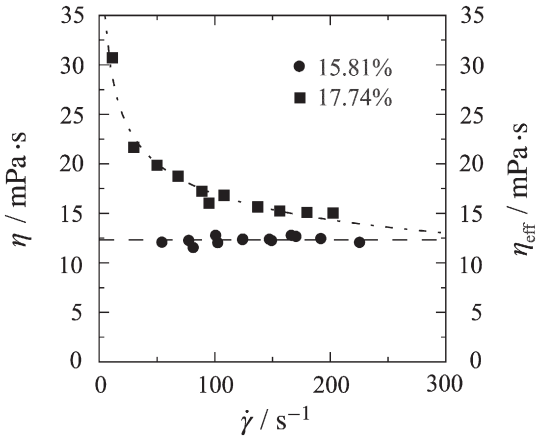


**Fig. 2.** Evidence of distinct of flow regimes: viscosity ($\eta$) and effective viscosity ($\eta_{\mathrm{eff}}$) as a function of shear rate ($\dot{\gamma}$) for 15.81% and 17.74% TS content, respectively, at a temperature of 323.15 K. The dashed lines represent the trend lines of each data set.

$$\eta(T,TS) = \eta_{H_2O}(T) \cdot \exp\left(f_\eta(TS) \cdot T^{e_\eta}\right) \tag{5}$$

with

$$f_\eta(TS) = a_\eta \cdot \left(\frac{TS}{100}\right) + b_\eta \cdot \left(\frac{TS}{100}\right)^2 + c_\eta \cdot \left(\frac{TS}{100}\right)^3 + d_\eta \cdot \left(\frac{TS}{100}\right)^4 \tag{6}$$

and where $\eta$ is the viscosity in mPa·s, $T$ is the temperature in K, $TS$ is the total solid content in %, and $\eta_{H2O}(T)$ is the viscosity of water in mPa·s calculated for temperature $T$ and atmospheric pressure using the IAPWS formulation of Huber et al. [40].

The experimental data in Table S2.2 (see Supporting Information) were fit with Eqs. (5) and (6) using the same approach as mentioned in Section 3.2; the resulting coefficients $a_\eta$, $b_\eta$, $c_\eta$, $d_\eta$ and $e_\eta$ are found

**Table 2**
Coefficients $a_i$, $b_i$, $c_i$, $d_i$, $e_i$ and $f_i$ for Eqs. (3), (5), (6), (8), (9), (11) and (12).

| $i$ | $a_i$ | $b_i$ | $c_i$ | $d_i$ | $e_i$ | $f_i$ |
|---|---|---|---|---|---|---|
| $\rho$ | 6939.24 | −0.61026 | −35.7589 | 4.89120 | 1.13287 | 1.01803 |
| $\eta$ | 0.03104 | −0.63028 | 6.05938 | −18.0001 | 1.28583 | – |
| $k$ | 0.93837 | 0.35426 | 3.20530 | 810.170 | −4.79170 | – |
| $n$ | −0.02109 | 125.198 | 0.50000 | 0.85769 | 16,437.0 | – |
| $c_p$ | −10,937.47 | 100,317.1 | −408,166.81 | 312,572.3 | −1.29592 | – |

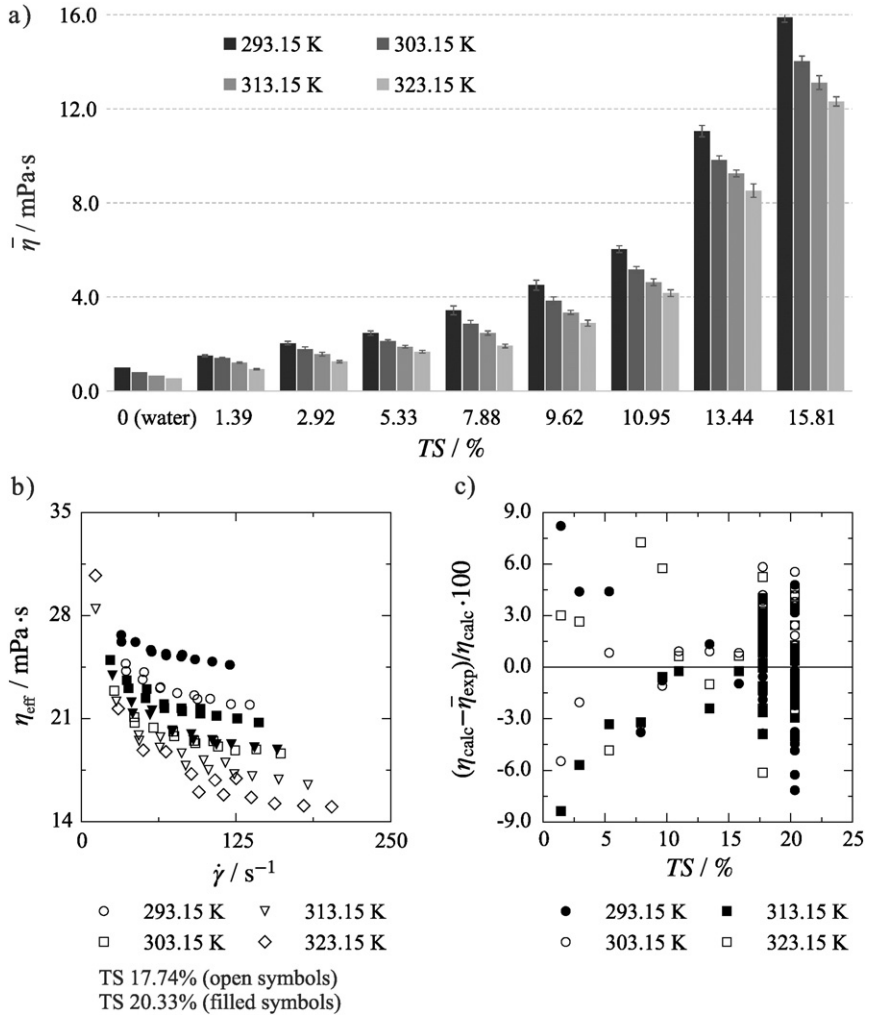


**Fig. 3.** Viscosity results: a) averaged viscosities ($\bar{\eta}$) for algae samples exhibiting Newtonian flow behavior as a function of temperature and TS content, and water viscosities calculated using the IAPWS formulation of Huber et al. [40] (shown for comparison), b) effective viscosities ($\eta_{eff}$) for 17.74% (open symbols) and 20.33% (filled symbols) TS content samples at various temperatures and as a function of shear rate ($\dot{\gamma}$), and c) percent deviations between experimental and calculated viscosities and effective viscosities using Eqs. (5) and (7), respectively, at various temperatures and as a function of TS content.

in Table 2. The relative deviations between experimental and calculated viscosities are presented in Fig. 3c; for all TS contents up to 15.81%, 95% of the data fall between ±5.8%. The largest deviations occur at the lowest TS content (1.42%), whereas the deviations are within ±2% for TS contents >10%.

The extrapolation behavior of Eq. (5) is plotted for TS contents from 0% to 16% and for temperatures from 274 K to 365 K in Fig. S3.1c and S3.1d in the Supporting Information, respectively. As was the case for density, it is clear from these plots that the equation exhibits normal trends without any unusual variations indicating that it is valid over the entire measurement range.

Schneider and Gerber [14] previously reported an equation for untreated, thermally pretreated, and digested algal biomass exhibiting non-Newtonian, shear-thinning behavior. They used the power-law model ($\tau = k\cdot\dot{\gamma}^n$), which is also known as the Ostwald-de Waele relationship. Thus,

$$\eta_{eff} = k\cdot\dot{\gamma}^{n-1} \tag{7}$$

represents the effective viscosity $\eta_{eff}$ as a function of the shear rate $\dot{\gamma}$, the flow consistency index, $k$, in Pa·s$^n$, and the dimensionless flow behavior index, $n$. The following equations were developed to calculate the indices $k$ and $n$ as functions of temperature and TS content:

$$k(T,TS) = a_k\cdot\left(b_k\cdot\frac{TS}{100}+\left(\frac{TS}{100}\right)^{c_k}\right)\cdot\left(d_k\cdot\frac{T/\mathrm{K}}{1000}+\left(\frac{T/\mathrm{K}}{1000}\right)^{e_k}\right) + \left(1-\frac{TS}{100}\right)\cdot\frac{\eta_{H_2O}(T)}{\mathrm{mPa\cdot s}}\,[\mathrm{Pa}\cdot s^n] \tag{8}$$

and

$$n(T,TS) = a_n\cdot\left(b_n\cdot\frac{TS}{100}+\left(\frac{TS}{100}\right)^{c_n}\right)\cdot\left(d_n\cdot\frac{T/\mathrm{K}}{1000}+\left(\frac{T/\mathrm{K}}{1000}\right)^{e_n}\right)+1 \tag{9}$$

In this study, the experimental data in Table S2.3 (see Supporting Information) were fit with Eqs. (8) and (9) using the least-squares method. However, only the linearly dependent coefficients $a_k$, $b_k$, $d_k$, $a_n$, $b_n$ and $d_n$ were fit, while the previously determined values [14] for exponents $c_k$, $e_k$, $c_n$ and $e_n$ were retained. This was done to constrain the equations since they were being fit to just two data sets. The resulting coefficients are reported in Table 2. The relative deviations between the experimental and calculated effective viscosities for the 17.74%

and 20.44% TS content samples predominantly (95%) range between ± 5.6% (Fig. 3c). The deviations for all TS contents (Newtonian and non-Newtonian) and temperatures are randomly distributed (Fig. 3c).

Finally, in Fig. S3.1e and S3.1f in the Supporting Information the extrapolation behavior of Eq. (7), in combination with Eqs. (8) and (9), is plotted as a function of shear rate over the range from 0 to 500 $s^{-1}$. Specifically, Fig. S3.1e shows the extrapolation behavior at constant temperature and increasing TS content, and Fig. S3.1f shows the extrapolation behavior at constant TS content and increasing temperature. Both figures demonstrate that the equation exhibits normal trends without any unusual variations.

### 3.4. Heat capacity

Table S2.4 in the Supporting Information summarizes the results of isobaric heat capacity measurements including corresponding expanded uncertainties. Reported heat capacity values are overall averages. As was previously discussed, for each TS content at least three samples were prepared and each of those samples was measured three times for a total of at least nine measurement runs per TS content. For a given TS content, replicate measurement results were averaged for each of the three measured samples and then those averages were compared to check for any evidence of mass-dependence; since no mass-dependence was observed, results were further averaged to give a single overall average as a function of temperature for each measured TS content.

Expanded uncertainties ($U(\overline{c_p})$) were calculated in a manner analogous to that previously described for density (Section 3.2). Here, the combined standard uncertainty for a single replicate measurement of a single sample mass can be expressed as

$$u(c_p) = \sqrt{\left(\frac{\partial c_p}{\partial K_{cp}}\right)^2 u^2(K_{cp}) + \left(\frac{\partial c_p}{\partial m}\right)^2 u^2(m) + \left(\frac{\partial c_p}{\partial c_{pm}}\right)^2 u^2(c_{pm})} \quad (10)$$

where the first term is the contribution from the uncertainty associated with the heat capacity calibration ($K_{cp}$), the second term is the contribution from the uncertainty in the sample mass ($m$), and the last term is the uncertainty associated with the measured heat capacity signal produced by the instrument ($c_{pm}$). The last term is a contribution of random and systematic sources of error and includes contributions associated with uncertainties in temperature and heat flow, among others. The combined standard uncertainty for a single sample mass is then calculated using propagation of errors to combine uncertainties for the three replicate runs. Finally, the combined standard uncertainty for each TS content can then be calculated using propagation of errors to combine uncertainties for each of the three measured masses. The Welch-Satterthwaite approximation [35] is used to calculate the effective degrees of freedom at each step of the calculation, and the final value is used to determine the appropriate coverage factor from a t-distribution for a 95% confidence level. Resulting expanded uncertainties ($U(\overline{c_p})$) and corresponding coverage factors ($k(df)$) are shown in Table S2.4 (see Supporting Information). Overall, expanded uncertainties range between 0.097 $J \cdot g^{-1} \cdot K^{-1}$ and 0.125 $J \cdot g^{-1} \cdot K^{-1}$ (2.6% to 3.1%).

It should be noted that the data presented in Table S2.4 represent a subset of the collected measurement data. Although measurement scans were performed from 278.15 K to 338.15 K, only data from the stable portion of the heat flow curves at approximately 298 K to 327 K are presented. Additionally, although data were collected at an approximate rate of one point every 0.4 s, the data were further reduced to a point every 1 K to make the amount of data presented in Table S2.4 more reasonable.

Averaged isobaric heat capacities are plotted as a function of temperature in Fig. 4a. Also shown in Fig. 4a is the heat capacity of water at atmospheric pressure calculated using the IAPWS-95 formulation of Wagner and Pruss [39]. It can be seen that $c_p$ decreases irregularly with increasing TS content. For instance, at a constant temperature of 313.13 K, a 2.5% increase of TS content from 5.33% to 7.87% results in a decrease in heat capacity of −0.81%, whereas a comparable increase in TS content from 10.95% to 13.44% leads to a decrease of −1.43%.

In contrast to what was observed for TS content, Fig. 4a shows a smooth temperature dependence for the isobaric heat capacity of *N. salina*. The $c_p$ decreases to a minimum and then increases almost linearly with temperature; this behavior can be attributed to the samples' aqueous content. Whereas the heat capacity of most other liquids rise continuously with temperature, liquid water has a shallow minimum between 303 K and 313 K [44] and the slope of the heat capacity changes from weakly negative to weakly positive with increasing temperature. However, Fig. 4a also shows that this minimum gets slightly more distinct with increasing TS content; at first glance, this seems counterintuitive. But, the same behavior was observed in a study by Darros-Barbosa et al. [45] that investigated the heat capacity of aqueous solutions of different sugars and salts as a function of temperature and water content. The authors attributed the observed behavior to changes in the structural composition of the samples at higher TS concentrations followed by dissolution. Thus, it is possible that the formation of flocs at higher TS contents is responsible for this behavior.

Correlations relating specific heat capacity, temperature, and total solid content are not available in the literature; once again, the only examples that could be found were for liquid foods. A good overview of these equations is given by Magerramov [46]. In most cases, simple polynomial equations were used and none of the equations accounted for the heat capacity of water at a TS content of 0%. In accordance with the equations found in the relevant literature, a numerically stable but accurate polynomial approach was chosen here. The following empirical equations were established to allow for the calculation of the isobaric heat capacity of *N. salina* algal biomass as a function of temperature and TS content:

$$c_p(T, TS) = c_{p,H_2O}(T) + f_{c_p}(TS) \cdot T^{e_{c_p}} \quad (11)$$

with

$$f_{c_p}(TS) = a_{c_p} \cdot \left(\frac{TS}{100}\right) + b_{c_p} \cdot \left(\frac{TS}{100}\right)^2 + c_{c_p} \cdot \left(\frac{TS}{100}\right)^3 + d_{c_p} \cdot \left(\frac{TS}{100}\right)^4 \quad (12)$$

where $c_p$ is the isobaric heat capacity in $J \cdot g^{-1} \cdot K^{-1}$, $T$ is the temperature in K, $TS$ is the total solid content in %, and $c_{p,H2O}(T)$ is the isobaric heat capacity of liquid water in $J \cdot g^{-1} \cdot K^{-1}$ at a given temperature and at atmospheric pressure. This last term was calculated using the IAPWS-95 formulation of Wagner and Pruss [39].

The experimental data were fit with Eqs. (11) and (12) and the resulting coefficients $a_{cp}$, $b_{cp}$, $c_{cp}$, $d_{cp}$ and $e_{cp}$ can be found in Table 2. Again, a Newton-Raphson method was used to reduce the weighted sum of squares for the adjustment of the equation parameters. Fig. 4b shows the relative deviations between experimental and calculated isobaric heat capacities. For clarity, deviations are shown for only select temperatures (every 4 K), as well as the minimum and maximum observed deviation at each TS content. Overall, 95% of the deviation data range between −0.47% and 0.50%. Furthermore, Fig. 4b shows no systematic offset and deviations that are randomly distributed for all TS contents and temperatures.

Finally, the extrapolation behavior of Eq. (11) is plotted for TS contents from 0% to 30% and for temperatures from 278 K to 368 K in Fig. S3.1g and S3.1h in the Supporting Information, respectively. The equation exhibits normal trends without any unusual variations.

## 4. Conclusion

Density, viscosity, and isobaric heat capacity of microalgae biomass (*Nannochloropsis salina*) were experimentally investigated as a function of temperature and TS content. While both density and viscosity increase with increasing TS content and decreasing temperature, heat

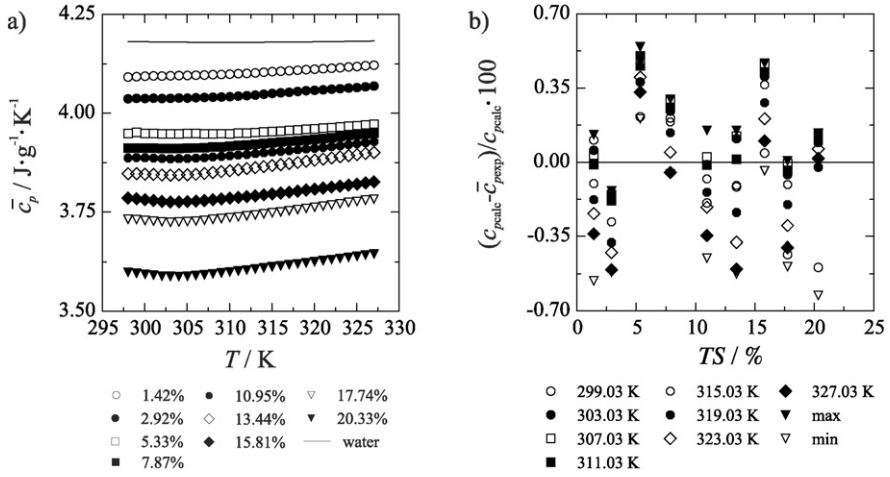


**Fig. 4.** Isobaric specific heat capacity ($c_p$) results: a) experimental results for measured TS concentrations plotted as a function of temperature ($T$) and values for pure water calculated using the IAPWS formulation of Wagner and Pruss [39], and b) percent deviations for experimental data relative to heat capacities calculated using Eq. (11). For a more complete picture, deviations are shown in 2 to 4 K steps for the whole temperature range as well as the minimum and maximum deviation at each TS content.

capacity decreases with increasing TS content and exhibits a more complicated temperature dependence. Specifically, heat capacity initially decreases slightly until a minimum is reached and then it increases with increasing temperature. Equations were developed that allow for the calculation of the investigated thermophysical properties as a function of temperature and TS content, thus providing a convenient way to estimate thermophysical properties of *N. salina* algal biomass at different conditions. Currently, the results of this work should be limited to *N. salina* biomass. One might assume that these results can be extended to other microalgae species that exhibit the same cell size and structure and a comparable organic and elemental composition as *N. salina*. However, additional experiments are needed to verify whether or not the equations presented herein can be applied to other microalgae species.

## Acknowledgements

This work was supported by the Ruhr University Research School PLUS, funded by Germany's Excellence Initiative [DFG GSC 98/3]. The authors thank Dr. Thomas J. Bruno of National Institute of Standards and Technology for supervising this work, Dr. Jessica Burger for her help with the FNR, Dr. Monika Thol of Ruhr-Universität Bochum for helpful discussions during the development of the correlation equations and Dr. Olga Reifschneider of Ruhr-Universität Bochum for her help with the microscopic analysis and helpful discussions regarding cell biology.

## Supporting Information

Supplementary data to this article can be found online at http://dx.doi.org/10.1016/j.fuproc.2016.06.039.

## References

[1] R. Harun, M. Singh, G.M. Forde, M.K. Danquah, Bioprocess engineering of microalgae to produce a variety of consumer products, Renew. Sust. Energ. Rev. 14 (2010) 1037–1047.
[2] S. Behera, R. Singh, R. Arora, N.K. Sharma, M. Shukla, S. Kumar, Scope of algae as third generation biofuels, Front. Bioeng. Biotechnol. 2 (2015) 1–13.
[3] T. Mata, A. Martins, N. Caetano, Microalgae for biodiesel production and other applications. A review, Renew. Sust. Energ. Rev. 14 (2010) 217–232.
[4] M.F. Demirbas, Biofuels from algae for sustainable development, App. Energ. 88 (2011) 3473–3480.
[5] A. Wileman, A. Ozkan, H. Berberoglu, Rheological properties of algae slurries for minimizing harvesting energy requirements in biofuel production, Bioresour. Technol. 104 (2012) 432–439.
[6] M. Santos, M. Martins, J. Coimbra, R. Gates, L. Corrêdo, Rheological behavior of *Chlorella* sp. e *Scenedesmus* sp. cultures in different biomass concentrations, Eng. Agrí. 33 (2013) 1063–1071.
[7] P. Wiley, E. Campbell, B. McKuin, Production of biodiesel and biogas from algae. A review of process train options, Water Environ. Res. 83 (2011) 326–338.
[8] Y. Chisti, Biodiesel from microalgae, Biotechnol. Adv. 25 (2007) 294–306.
[9] X. Zhang, Z. Jiang, L. Chen, A. Chou, H. Yan, Y. Zuo, X. Zhang, Influence of cell properties on rheological characterization of microalgae suspensions, Bioresour. Technol. 139 (2013) 209–213.
[10] M. Michels, A. van der Goot, N. Norsker, R. Wijffels, Effects of shear stress on the microalgae *Chaetoceros muelleri*, Bioprocess Biosyst. Eng. 33 (2010) 921–927.
[11] F. Chen, H. Chen, X. Gong, Mixotrophic and heterotrophic growth of *Haematococcus lacustris* and rheological behaviour of the cell suspensions, Bioresour. Technol. 62 (1997) 19–24.
[12] V. Adesanya, D. Vadillo, M. Mackley, The rheological characterization of algae suspensions for the production of biofuels, J. Rheol. 56 (2012) 925–939.
[13] A. Souliès, J. Pruvost, J. Legrand, C. Castelain, T. Burghelea, Rheological properties of suspensions of the green microalga *Chlorella vulgaris* at various volume fractions, Rheol. Acta 52 (2013) 589–605.
[14] N. Schneider, M. Gerber, Correlation between viscosity, temperature and total solid content of algal biomass, Bioresour. Technol. 170 (2014) 293–302.
[15] M. Bartley, W. Boeing, A. Corcoran, F. Holguin, T. Schaub, Effects of salinity on growth and lipid accumulation of biofuel microalga *Nannochloropsis salina* and invading organisms, Biomass Bioenerg. 54 (2013) 83–88.
[16] H. Greenfield, D. Southgate, Food Composition Data - Production, Management and Use, Food and Agriculture Organisation of the United Nations (FAO), Rome, Italy, 2003.
[17] Water Chemistry Society, German Standard Methods for Examination of Water, Wastewater and Sludge, Wiley-VCH, Weinheim, Germany, 2014.
[18] T.J. Fortin, Assessment of variability in the thermophysical properties of rocket propellant RP-1, Energ. Fuel 26 (2012) 4383–4394.
[19] A. Laesecke, T.J. Fortin, J.D. Splett, Density, speed of sound, and viscosity measurements of reference materials for biofuels, Energ. Fuel 26 (2012) 1844–1861.
[20] T.J. Fortin, A. Laesecke, M. Freund, S. Outcalt, Advanced calibration, adjustment, and operation of a density and sound speed analyzer, J. Chem. Thermodynamics 57 (2013) 276–285.
[21] H. Yamamoto, K. Kamawura, K. Omura, S. Tokudome, Development of a compact-sized falling needle rheometer for measurement of flow properties of fresh human blood, Int. J. Thermophys. 31 (2010) 2361–2379.
[22] H. Yamamoto, K. Kamawura, K. Omura, S. Tokudome, Development of a compact-sized falling needle rheometer for measurement of flow properties of fresh human blood, 17th Symposium on Thermophysical Properties, Boulder, CO, USA, 2009.
[23] N.A. Park, T.F. Irvine, The falling needle viscometer - a new technique for viscosity measurements, Heat Mass Transf. 18 (1984) 201–206.
[24] N.A. Park, T.F. Irvine, Measurements of rheological fluid properties with the falling needle viscometer, Rev. Sci. Instruments 59 (1988) 2051–2058.
[25] D.S. Viswanath, T. Ghosh, D.H.L. Prasad, N.V.K. Dutt, K.Y. Rani, Viscosity of Liquids - Theory, Estimation, Experiment and Data, Springer Netherlands, Dordrecht, Netherlands, 2007.
[26] J. Burger, H. Yamamoto, T. Suzuki, A. Laesecke, Application of falling-needle rheometry to highly concentrated DNA solutions, Biorheology 51 (2014) 29–45.
[27] M. Reading, A. Luget, R. Wilson, Modulated differential scanning calorimetry, Thermochem. Acta 238 (1994) 295–307.
[28] B. Wunderlich, Y. Jin, A. Boller, Mathematical description of differential scanning calorimetry based on periodic temperature modulation, Thermochem. Acta 238 (1994) 277–293.

[29] G.J. Rosasco, J.R. Whetstone, R.L. Watters, Certificate of Analysis – Standard Reference Material 2232, National Institute of Standards and Technology, Gaithersburg, MD, USA, 2003.
[30] S.D. Rasberry, Certificate of Analysis – Standard Reference Material 2220, National Institute of Standards and Technology, Gaithersburg, MD, USA, 1989.
[31] E.F. Westrum, The thermophysical properties of three globular molecules, J. Phys. Chem. Solids 18 (1961) 83–85.
[32] D.G. Archer, Thermodynamic properties of synthetic sapphire (a-Al2O3), standard reference material 720 and the effect of temperature-scale differences on thermodynamic properties, J. Phys. Chem. Ref. Data 22 (1993) 1441–1453.
[33] L. Christenson, R. Sims, Production and harvesting of microalgae for wastewater treatment, biofuels, and bioproducts, Biotechnol. Adv. 29 (2011) 686–702.
[34] S. Schwede, A. Kowalczyk, M. Gerber, R. Span, Anaerobic co-digestion of the marine microalga *Nannochloropsis salina* with energy crops, Bioresour. Technol. 148 (2013) 428–435.
[35] International Organization for Standardization (ISO), Guide to the Expression of Uncertainty in Measurement, ISO, Geneva, Switzerland, 1995.
[36] A.M. Ramos, A. Ibarz, Density of juice and fruit puree as a function of soluble solids content and temperature, J. Food Eng. 35 (1998) 57–63.
[37] A. Mohamadi Sani, G. Hedayati, A. Arianfar, Effect of temperature and concentration on density and rheological properties of melon (*Cucumis melo* L. var. *Inodorus*) juice, Nutrition & Food Science 44 (2014) 168–178.
[38] A.L. Gabas, R.A.F. Cabral, C.A.F. Oliveira, J. Telis-Romero, Density and rheological parameters of goat milk, Food Sci. Technol. (Campinas) 32 (2012) 381–385.
[39] W. Wagner, A. Pruss, The IAPWS formulation 1995 for the thermodynamic properties of ordinary water substance for general and scientific use, J. Phys. Chem. Ref. Data 31 (2002) 387–535.
[40] M. Huber, R. Perkins, A. Laesecke, D. Friend, J. Sengers, M. Assael, I.N. Metaxa, E. Vogel, R. Mareš, K. Miyagawa, New international formulation for the viscosity of water, J. Phys. Chem. Ref. Data 38 (2009) 101–125.
[41] H.A. Barnes, A Handbook of Elementary Rheology, University of Wales, Institute of Non-Newtonian Fluid Mechanics, Aberystwyth, Wales, 2000.
[42] Z. Wu, X. Shi, Rheological properties of *Chlorella pyrenoidosa* culture grown heterotrophically in a fermentor, J. Appl. Phycol. 20 (2008) 279–282.
[43] F. Fernández-Martín, Influence of temperature and composition on some physical properties of milk and milk concentrates. II. Viscosity, J. Dairy Res. 39 (1972) 75–82.
[44] K. Trincher, The mathematic-thermodynamic analysis of the anomalies of water and the temperature of life, Water Res. 15 (1981) 433–448.
[45] R. Darros-Barbosa, M. Balaban, A. Teixeira, Temperature and concentration dependence of heat capacity of model aqueous solutions, Int. J. Food Prop. 6 (2003) 1–20.
[46] M. Magerramov, Heat capacity of natural fruit juices and of their concentrates at temperatures from 10 to 120 °C, J. Eng. Phys. Thermophys. 80 (2007) 1055–1063.